Journal of Membrane Science and Research 5 (2019) 222-232

Journal of Membrane Science & Research

journal homepage: www.msrjournal.com

Research Paper

Polysulfone Ultrafiltration Membranes Modified with Carbon-Coated Alumina Supported Ni-TiO_2 Nanoparticles for Water Treatment: Synthesis, Characterization and Application

Bhekani S. Mbuli, Mphilisi M. Mahlambi, Catherine J. Ngila, Richard M. Moutloali *

Department of Chemical Sciences, University of Johannesburg, P.O. Box 17011, Doornfontein, 2028, Johannesburg, South Africa
DST/Mintek Nanotechnology Innovation Centre - Water Research Node, Private Bag X3015, Randburg, 2125, South Africa

Article info

Received 2018-01-25
Revised 2018-05-09
Accepted 2018-05-25
Available online 2018-05-25

Keywords

Carbon coated alumina
TiO_2 nanophotocatalyst
Mixed matrix membrane
Polysulfone

Highlights

- Incorporation of CCA/Ni-TiO_2 nanoparticles improved water permeability of the modified membranes
- Salt and heavy metal rejection of the mixed matrix membranes improved due to electrostatic effects of the nanoparticles
- Mixed matrix membranes had improved photocatalytic activity towards bromophenol blue than methyl orange through a pseudo-first-order reaction rate

Graphical abstract

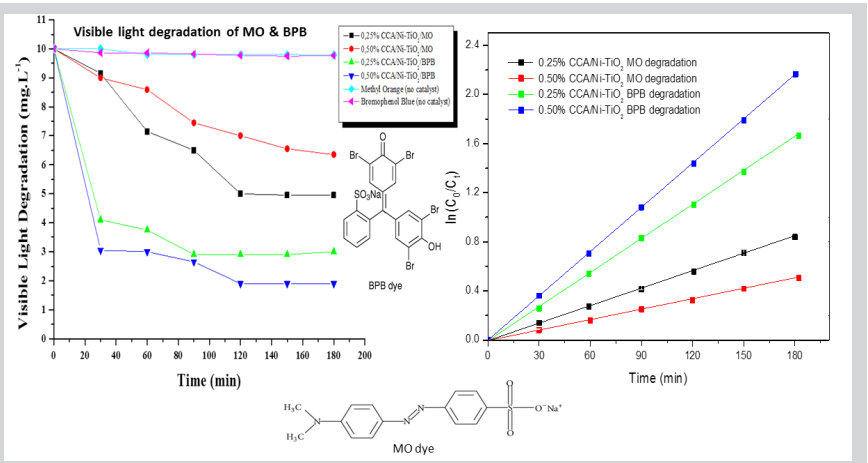

Abstract

This paper reports on the synthesis and characterisation of polysulfone (PSf) ultrafiltration (UF) membranes modified with carbon coated alumina Ni-doped titanium dioxide (CCA/Ni-TiO_2) nanoparticles. The syntheses of the membranes was carried out using the phase inversion process. The permeate flux of the membrane modified with 0.25% CCA/Ni-TiO_2 nanoparticles (213.5±6.40 $L.m^{-2}.h^{-1}$) was found to be higher than that of the unmodified membrane (130.95±4.50 $L.m^{-2}.h^{-1}$) at 13.8 bar. The membrane modified with 0.50% CCA/Ni-TiO_2 nanoparticles had the lowest permeate flux at 105.18±4.52 $L.m^{-2}.h^{-1}$. The improved water permeability was brought about by the hydrophilicity resulting from introduction of the hydroxyl groups of the nanoparticles. At 13.8 bar, the NaCl salt rejection properties of the mixed matrix membranes were relatively higher (31.38±1.23%) for the 0.25% PSf/CCA/Ni-TiO_2 membranes compared to that of the unmodified PSf membrane (12.76±1.10%). Similar observations were made for the Cr^{3+} heavy metal rejection, which ranged between 56.27±2.54% and 60.48±2.52% for the modified membranes. These results have demonstrated the role the electrostatic effects of the nanoparticles play in the rejection mechanism of the modified membranes when compared to the unmodified membranes. Unmodified membranes were found to reject 28.32±1.65% of Cr^{3+} heavy metals at the same pressure. Over a period of 180 minutes, the membranes were found to be more photocatalytically active towards bromophenol blue, and a maximum photodegradation efficiency of 81% was achieved compared to only 50.5% for methyl orange. The photo-degradation process for both dyes followed a pseudo-first-order reaction rate.

1. Introduction

Chromium (Cr) is widely used in various industrial applications such as electroplating, alloying, pigment fixation and corrosion tutelary films [1]. Although Cr exists in several chemical forms with oxidation numbers ranging from 0 to 6, the two most common oxidation states of Cr present in the environment are the trivalent and hexavalent forms. The di-, tetra- and penta-valent oxidation forms are unstable and are often rapidly converted to the trivalent (Cr^{3+}) form, which is in turn converted to the hexavalent (Cr^{6+}) form. Cr^{6+} is carcinogenic, and therefore, requires removal from wastewater effluent [2]. Other than being the most oxidation form abundant in natural water systems, Cr^{3+} is also mainly discharged by the metal industry. Cr^{3+} can under suitable conditions such as the presence of strong oxidising agents be easily converted to Cr^{6+}. An investigation of the removal of Cr^{3+} from aqueous media, which is the focus of this study, is important since Cr^{3+} is perceived as the precursor of the much more toxic Cr^{6+} [2, 3].

Cr^{3+} ions are biologically essential because of the vital role they play in the metabolism of nucleic acid, lipids, proteins and vitamin B12. However, it should be noted that excessive amounts of Cr^{3+} ions can potentially enhance the toxicity of Cr^{3+} ions [1]. For example, Cr^{3+} has been shown to lead to

* Corresponding author at: Phone: +27 (0) 11 559 6885; Fax: +27 (0) 11 559 6425
E-mail address: rmoutloali@uj.ac.za (R.M. Moutloali)

DOI: 10.22079/JMSR.2018.80046.1173

thyroid damage, slowed respiration, permanent disability and decreased pulmonary function in animals [1]. In plants, Cr^{3+} is required in trace amounts as it promotes plant productivity. Unfortunately, Cr^{3+} can also cause seed germination delays as well as reduced photosynthesis and biomass. Excessive amounts of Cr^{3+} in plants can also lead to chlorosis, necrosis and death of crops. Antagonistic interference may also occur in the presence of essential nutrients such as calcium, iron, phosphorus, potassium, manganese, zinc and copper [3]. Such interference may affect the metabolic processes of the plant *via* oxidative stress, which causes chloroplast and pigment alterations. Cr^{3+} ions can also suppress the function and regulation of several proteins such as antioxidant enzymes, which are responsible for chromosomal impairments in plant tissues [4]. Since the release of Cr^{3+}-based pollutants into the environment can pose a threat to aquatic life due to their toxicities, an attempt to remove them from contaminated water was undertaken in this research study. The removal of the Cr^{3+} pollutant was performed by using carbon-coated alumina coupled with TiO_2 nanoparticle modified membranes.

Moustakes et al. (2014) reported that industrial effluents from textile industries contain salts that are co-dissolved with dyes [5]. This clearly demonstrates that the removal of dissolved salts from wastewater co-dissolved with dyes remains a grave concern in industrial effluents. Traditionally, dissolved NaCl salts are commonly removed from wastewater by reverse osmosis (RO) and nanofiltration (NF) membranes. However, RO/NF membrane technologies tend be more expensive. The aim of this research was, therefore, to determine the efficiency of ultrafiltration membranes (UF) modified with carbon coated alumina (CCA) Ni-TiO_2 nanoparticles that possess dye degrading properties towards the removal of dissolved salts from dye containing wastewater.

Traditionally, researchers explained the rejection capacity of UF membranes on the basis of the Donnan Size Exclusion principle as the dominant mechanism for the extraction of pollutants [5]. It is generally believed that Donna Size Exclusion effect on dissolved salts is minimal in ultrafiltration membranes. On the contrary, recent reports have shown that other mechanisms of electrostatic interaction origin play a significant role in the rejection of dissolved monovalent and divalent salts by ultrafiltration membranes [6]. Therefore, this research work is intended to explore the effects of electrostatic interactions between NaCl salts and modified PSf UF membranes. Such interactions will then be compared with similar interactions between the NaCl salts and the unmodified membrane. The NaCl solute was chosen because of its small size that will enable not to be rejected via the Donnan Size Exclusion mechanism [6].Therefore, the hypothesis was that if the small-sized NaCl salts can be rejected in considerable amounts by UF membranes, the rejection can clearly demonstrate that other rejection mechanisms such electrostatic interactions are effective in the UF membranes removal mechanism.

Ultrafiltration membrane processes are known to depend on the porosity, density and presence of functional groups in their membrane surfaces [7, 8]. These properties may influence both the physico-chemical changes inside the pore structure and the surface barriers such as surface charges, electrostatic properties and hydrophilicity. For example, macropores in the membrane matrix serve as transport pathways that yield high specific surface areas and allow fast permeation [9]. UF membranes utilize a pressure driven membrane separation process that takes into consideration the size exclusion effect, Donnan exclusion, and physico-chemical properties of membrane polymer [10-12]. Water permeability and selectivity of membranes are controlled by concentration polarization due to the enhancement of the concentration of the rejected species on the membrane surface as a function of transmembrane flow [8, 9]. This phenomenon may reduce the performance of the membrane. However, to counter this challenge of low selectivity and water permeability, the membrane material can be modified to suit the environmental requirements. This means that the membrane can be modified in order to suit the specific water matrix to be treated [3, 12].

The commonly used polymer materials (polysulfone (PSf) and polyethersulfone (PES)) utilized for making ultrafiltration (UF) membranes are known to be slightly hydrophobic. Consequently, the membranes are prone to fouling, thus lowering their water permeability with prolonged usage. Membrane separation is based on the performance of the membranes, which is determined by its selectivity and productivity [13-16]. Modification of UF polymeric membranes becomes imperative when attempting to improve water permeability, while simultaneously maintaining relatively high selectivity. Surface charge, roughness, hydrophilicity, molecular-weight-cut-off, pore size and distribution are the main aspects that impose a great impact on the performance of membranes [13-16]. These membrane properties can be altered by modifying membrane surfaces with specific functional groups from different kinds of additives. For this reason, much research has been dedicated to the modification of UF membranes with additives such as nanoparticles (TiO_2, ZnO and Al_2O_3) and hydrophilic polymers (cyclodextrins and poly(ethyl glycol)) [16-21]. The incorporation of nano-sized materials into different types of materials can produce synergistic effects. Surface chemistry of metal oxides (Al_2O_3, TiO_2, ZrO_2 and SiO_2) has been shown to be directly controlled by the surface structure of the membranes. For instance, acid-base sites create metal cations and oxygen anions [18-27].

Previous research work in our laboratory has reported that under visible light, Rhodamine B dye can be degraded by CCA-supported titania (CCA/TiO_2) nanoparticles [28]. These CCA/TiO_2 nanoparticles completely degraded 100 mL (10 mg L^{-1}) within 180 minutes compared to 20.0% in a period of 300 minutes for unsupported TiO_2 nanoparticles under visible light. The Ni-TiO_2/CCA nanoparticles were shown to degrade 75.0% of Rhodamine B [29]. The CCA/Ag-TiO_2 was found to degrade 98.0% of the Rhodamine B after 300 minutes and 78.0% Rhodamine B degradation was achieved when CCA/Co-TiO_2 was employed [28, 29]. The dopants on these nanophotocatalysts improved their photocatalytic activity when compared with the un-doped and unsupported nanophotocatalysts. This was as a result of increased mean pore diameter of the doped nanoparticles relative to the un-doped nanoparticles. For example, the CCA/Ni-TiO_2 nanoparticles were found to possess surface area of 121 m^2 g^{-1}, total pore volume of 0.239 cm^3 g^{-1} and mean pore diameter of 6.48 nm. All these parameters were higher than those of the CCA/TiO_2 nanoparticles (surface area of 149 m^2 g^{-1}; total pore volume of 0.210 cm^3 g^{-1}; and mean pore diameter of 5.69 nm). Even though the surface area of doped nanoparticles were reduced and total pore volume remained the same, the mean pore diameter increased. This increase indicated an increased interaction platform where the catalyst and pollutant could realise improved photocatalytic activity [28, 29]. The band gap of the CCA/Ni-TiO2 nanoparticles was found to be 2.82 nm, which enhanced the visible light band edge of the photocatalyst. Moreover, the CCA/Ag-TiO_2 degraded the Rhodamine B much more effectively because it absorbed more of the visible light, resulting in higher degradation efficiency [28, 29]. Furthermore, these nanocomposites performed better than the unsupported TiO_2 nanoparticles in the degradation studies. Although these composites have shown great potential in the photodegradation of Rhodamine B, they lack an appropriate and robust support system. This has been a great challenge for the optimum utilization of these nanocomposites because it becomes difficult to separate them from the wastewater after being treated. The other challenge with such nanocomposites had always been leaching, whenever they are embedded in UF membranes. Hence, this study focused on immobilising the nanocatalysts on carbon coated alumina to make nanocomposites, prior to being incorporated into the PSf UF membrane support system. This was envisaged to improve the support system of the nanocomposites on membranes that could lead to their optimal use in water treatment.

In a study undertaken by Mahlambi et al. [28], novel polysulfone supported 0.50% CCA/TiO_2 mixed matrix membranes were synthesized and found to possess a permeate flux of 164 $L.m^{-2}.h^{-1}$ at a pressure of 1 bar. The same membranes were found to reject between 81.0% and 96.0% of Rhodamine B dye following anchoring of the CCA/TiO_2 on the polysulfone membranes [28]. This anchoring of the CCA/TiO_2 nanoparticles onto the membranes was found to be better in terms of rejection performance than unmodified PSf UF membranes. Such a concept shows great potential of the nanocomposites when supported on UF membranes, because of the resultant higher permeate flux and rejection capacities. However, this research study was limited to the incorporation of CCA/TiO_2 nanoparticles. Hence, the study had to be extended into the other well-performing nanophotocatalysts on UF membranes. The aim of this study was therefore to determine how the incorporation of the nanophotocatalysts onto UF membrane support systems influences the water permeability, rejection and degradation properties of the resultant UF membranes.

A lot of research has been carried out on the application of PSf UF membrane modified with TiO_2 nanophotocatalysts, and challenges such as leaching and reduced photocatalytic activity of the supported nanophotocatalysts have to this end been identified [19-25]. However, limited research involving the use of TiO_2 nanophotocatalysts immobilized with carbon coated alumina supports for use in PSf UF membrane systems have not been undertaken. The effect of these carbon coated alumina supports of Ni-TiO_2 nanoparticles on the rejection and permeate flux properties of the resultant polymeric UF membranes has also not been explored. Therefore, it was envisaged that the use of carbon coated alumina support would lead to the development of an improved support system for the TiO_2 nanocatalysts. This new support system will thereafter be incorporated onto the PSf UF membrane. Therefore, this research study sought to incorporate the immobilized CCA/Ni-TiO_2 nanocatalysts onto PSf UF membranes using the phase inversion process for application in water treatment. A study of the surface characteristics as well as the morphological, water permeability and rejection performance properties of the novel PSf/CCA/Ni-TiO_2 mixed matrix membranes will also be undertaken.

2. Materials and Methods

2.1. Materials

The reagents were obtained from relevant suppliers and used without further purification. 85.0 wt% 1-methyl-2-pyrrolidone (NMP) and polysulfone pellets were obtained from Sigma-Aldrich, South Africa. The non-woven fabric was sourced from Hirose Co., Japan.

2.2. Experimental

2.2.1. Synthesis of modified nanoparticles

The synthesis of CCA/Ni-TiO_2 nanoparticles was carried out according to an experimental procedure reported by Mahlambi et al. [29].

2.2.2. Synthesis of CCA/TiO_2/PSf membranes

The synthesized CCA/Ni-TiO_2 nanoparticles were dispersed in NMP as shown in Table 1. Small portions of polysulfone (PSf) pellets were added slowly and under stirring conditions to the reaction mixture. The polymeric mixture was allowed to react for 8 h and thereafter allowed to settle for 2 h. This mixture was then cast on a non-woven fabric fixed on a clean glass plate. A casting knife with a blade height set at 150 µm was used. The glass plate was immediately immersed in a coagulation bath containing an ice-deionised water mixture (0°C) for a period of 15 min. The resultant ultrafiltration membranes were then rinsed three times with clean deionised water and thereafter stored at 4.0°C in a refrigerator prior to use.

Table 1
Specific casting solution composition used for ultrafiltration membranes.

Membrane	CCA/Ni-TiO_2 (wt.%)	PSf (wt.%)	NMP (wt.%)
1	0.50	16.00	84.00
2	0.25	16.00	84.00
3	0.00	16.00	84.00

2.3. Characterization

2.3.1. Attenuated total reflectance-infrared (ATR-IR) spectroscopy

Attenuated total reflectance-infrared spectroscopy (ATR-IR) spectra of all the membranes were collected on a Perkin Elmer, Spectrum 100, spectrophotometer equipped with a diamond-germanium-selenium crystal. The angle of incidence was fixed at 45º to give a probing depth of the membranes of about 0.40 µm in the infra-red region. Dry specimen of membrane samples were mounted on the crystal with the active layer facing the crystal surface in such a way that good contact is made between the sample and the crystal surface.

2.3.2. RAMAN analysis

A Perkin Elmer RAMAN Micro 200 instrument was used for all RAMAN analyses. The instrument was equipped with a 785 nm laser lamp and had a maximum output of 250 mW. For analyses, the sample was placed on a quartz slide. After focusing the instrument to obtain the best image and then switched to the dark field, a light beam was then passed through the sample and the spectra were recorded.

2.3.3. Scanning electron microscope

A VEGA3 TESCAN scanning electron microscope was used to determine the surface and cross-section morphology of the mix-matrix membranes. The UF PSf membranes were frozen in liquid nitrogen and fractured to analyse the cross-section of the UF membranes. The membranes were mounted on a carbon tape and thereafter carbon coated prior to analyses.

2.3.4. Atomic force microscopy measurements

Atomic force microscopy (AFM) analyses of the composite membranes were carried out to determine the quantitative surface roughness of the samples using a Nanoscope 3D Multimode purchased from Veeco Instruments Inc. This instrument utilises SNL cantilevers (Veeco) with a spring constant of 0.12 Nm^{-1} through the contact mode in dry air. For best viewing of the specimen, AFM analyses were undertaken at appropriate magnification and focusing following a 12 h drying of the samples in a vacuum oven. The projection area used for the membranes was 30 µm x 30 µm.

2.3.5. Contact angle measurements

Contact-angle (CA) measurements were carried out using a Dataphysics Contact Angle Instrument (SCA 20, OCA 15EC) and a sessile drop method. Sessile droplets of deionised water were dislodged at room temperature onto the dry surfaces of the membranes. Five seconds after depositing the water droplet onto the sample, images were captured prior to measurements of the CA. Five measurements at different locations of the membrane sample were taken and averaged out to obtain the CA of the membrane.

2.4. Water uptake analysis

The wet weights of the membranes were determined by soaking the membranes in distilled water for 48 h and thereafter weighing them after they been mopped with blotting paper. The dry weights of the membranes were determined once the wet samples had been dried in an oven at 60ºC for 48 h. The percentage of the water content was obtained using Equation 1.

$$Water\ \ content\,(\%) = \left(\frac{W_0 - W_1}{W_0}\right) \times 100 \tag{1}$$

where, W_0 and W_1 are the weights of wet and dry membranes (in g), respectively.

2.5. Permeation and rejection studies of membranes

The pure water flux through the membranes was determined using a cross-flow system (Sterlitech™ membrane test cell system) for bench-scale water filtration experiments. Each membrane type was tested in triplicate. To achieve a constant flux, both the unmodified and modified membranes were compacted with deionised water for 6 h at a pressure of 30 bar. The permeate flux of the membranes was thereafter measured at 13,8 bar, 20,7 bar and 27,6 bar. The permeate flux (J_w) was calculated according to Equation 2 shown below.

$$J_w = \frac{V}{A \times t} \tag{2}$$

where, V (L) is the volume of water collected at time t (h) and A was the active surface area (m^2) of the membrane.

The rejection of the NaCl salt (2.00 g L^{-1}) and Cr^{3+} (2.00 g L^{-1}) were measured using a conductivity meter (using the conductivity as a concentration of ions dissolved in water). The NaCl salt was used to study the electrostatic interactions between the PSf UF membrane surfaces and the dissolved salt [43]. The rejection (R) of the NaCl was calculated by using Equation 2 as follows:

$$R = 100 \times \left(1 - \frac{C_p}{C_f}\right) \tag{3}$$

where, C_p is the solute concentration of the permeate stream, and C_f is the solute concentration of the feed solution.

2.6. Photodegradation analysis using visible light

The modified PSf UF membranes were tested for their ability to photodegrade methyl orange and bromophenol blue under visible light. The degradation of methyl orange and bromophenol blue by the modified PSf UF membranes were monitored using a Newport 9600 Full Spectrum Solar Simulator. A 150 W ozone free xenon lamp, which was used in this solar simulator instrument, produces a collimated beam of 33 mm in diameter that is equivalent to 1.33 suns. In order to exclude UV light exposure and thus

ensure that photodegradation was due to visible light irradiation, a GG420 UV filter was placed between the light source and reaction vessel containing the membrane and pollutant. The distance between the light source and the reaction vessel was set at 10 cm to produce a beam power equivalent to 1 sun. To reduce the effect of thermolysis of the dye pollutant, the reaction was conducted inside a jacketed beaker containing an inlet and outlet to allow water to be passed through the jacketed beaker so as to maintain the reaction temperature at room temperature. The photocatalytic activity of the PSf UF membranes towards 100 mL of each methyl orange and bromophenol blue dye solution with a concentration of 10 mg L^{-1}.

Typically, a 5 cm × 5 cm membrane was immersed in the relevant dye solution and stirred in the dark for 1 h so as to establish an adsorption−desorption equilibrium. The solution mixture was then irradiated with visible light and 2 mL aliquots were sampled at 30 min intervals. To determine the extent of photodegradation, the aliquots were analyzed at 554 nm using a Shimadzu UV-2450 UV−Vis spectrophotometer. All the photodegradation experiments were carried out in the dark room. The experiments were carried out in triplicates and the average value was reported.

3. Results and Discussion

3.1. ATR-FTIR analysis

The ATR-FTIR spectra of the 0.25% PSf/CCA/Ni-TiO_2 and 0.5% PSf/CCA/Ni-TiO_2 modified membranes were compared to that of the unmodified membranes. As shown in Figure 1, all three membranes studied exhibited bands typical of PSf membranes [30, 31]. New FTIR bands appearing at 1678 cm^{-1} and 1724 cm^{-1} were observed on the spectra of modified membranes thus suggesting a chemical interaction between the TiO_2 nanocatalyst and the PSf polymer component. Such peaks as well as with those observed at 1498 and 1510 cm^{-1} are typical of the –OH functional group of the TiO_2 nanocatalyst [30-33]. These peaks were not observed on the spectrum of the pristine membrane; this is indicative of the successful incorporation of the CCA/Ni-TiO_2 catalyst onto the PSf UF membrane.

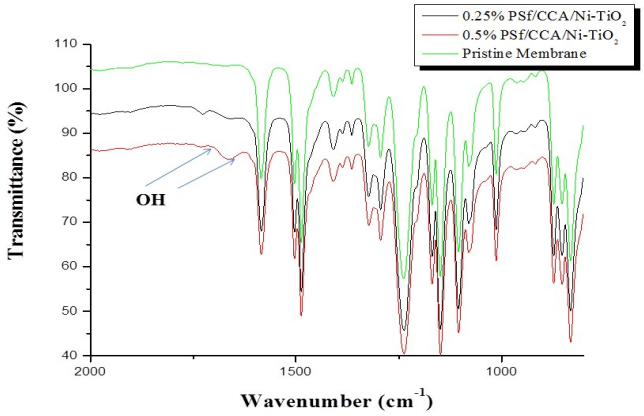

Fig. 1. ATR-FTIR spectra for the pristine, 0.25% and 0.50% PSf/CCA/Ni-TiO_2 UF membranes (arrows indicate the major bands associated with the TiO_2 nanocatalyst)

3.2. *RAMAN analysis*

Peaks associated with the pure PSf polymeric matrix, the Ni-TiO_2 as well as the carbon-covered alumina were observed in the RAMAN spectra of the pristine PSf and modified PSf/CCA/Ni-TiO_2 UF membranes (see Figure 2). The observed PSf RAMAN modes are in agreement with those reported in the literature [34, 35]. While the C–H stretching modes were found to appear at 3085.5 cm^{-1}, vibrations associated with the phenyl ring were observed at 1610.2 cm^{-1} and 1724.8 cm^{-1}. Both the strong C–O–C symmetric stretching mode and its corresponding weak asymmetric mode were observed at 1159 cm^{-1} and 1208.6 cm^{-1}, respectively. The peaks appearing at 1019.5 cm^{-1} and 1109.6 cm^{-1} were ascribed to the respective symmetric and asymmetric stretching modes of the $–SO_2$. At 634.8 cm^{-1}, an asymmetric –C–S–C stretching mode was observed and this was due to the out-of-plane benzene ring –C–H deformation that was observed at 790.2 cm^{-1}. It is evident from Figure 2 that the presence of the CCA/Ni-TiO_2 nanoparticles within the membrane matrix appears to have shifted some of the RAMAN bands to lower wavenumbers. Such a band shift suggests chemical bonding between the PSf and the CCA/Ni-TiO_2 nanoparticles.

The RAMAN modes associated with the Ni-TiO_2 nanoparticles, which are circled and shown as an insert in Figure 2a, and are in agreement with RAMAN shifts reported in previous studies [28]. However, the RAMAN modes of the anatase phase of the titania nanoparticles appear to be subdued due to the higher composition of the nanoparticles relative to the polymer. As shown in Figure 2b, the D (1298.7 cm^{-1}) and G (1461.9 cm^{-1}) carbon bands (see insert), which provide evidence for the presence of carbon in the CCA/TiO_2 nanoparticles, were observed. While the G band is due to bond stretching of the sp^2 carbon atoms, the D (disorder) band is attributable to the breathing modes of the sp^2 carbon atoms in the ring. Therefore, results of the RAMAN analysis confirmed the successful incorporation of the CCA/Ni-TiO_2 nanoparticles into the PSf polymeric membrane matrix.

3.3. Morphological studies

3.3.1. Scanning electron microscopy and EDS studies

Figure 3 shows both the surface and the cross-sections of the different membranes and their corresponding EDS spectra. The presence of Ni-TiO_2 nanomaterials on the surfaces of the modified membranes, which was confirmed by an analysis of the corresponding EDS spectra, is clearly evident in Figures 3b and c.

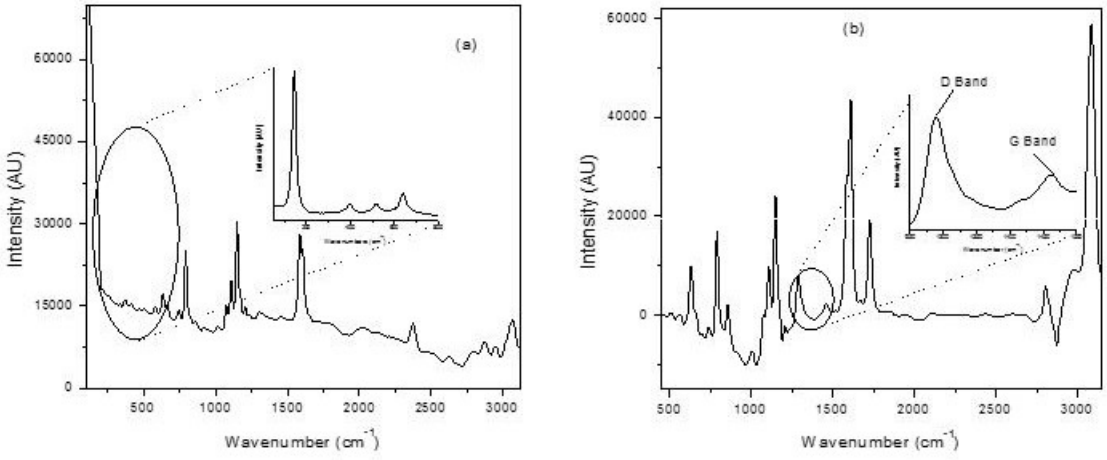

Fig. 2. RAMAN spectra of (a) pristine PSf and (b) modified PSf/CCA/Ni-TiO_2 UF membranes.

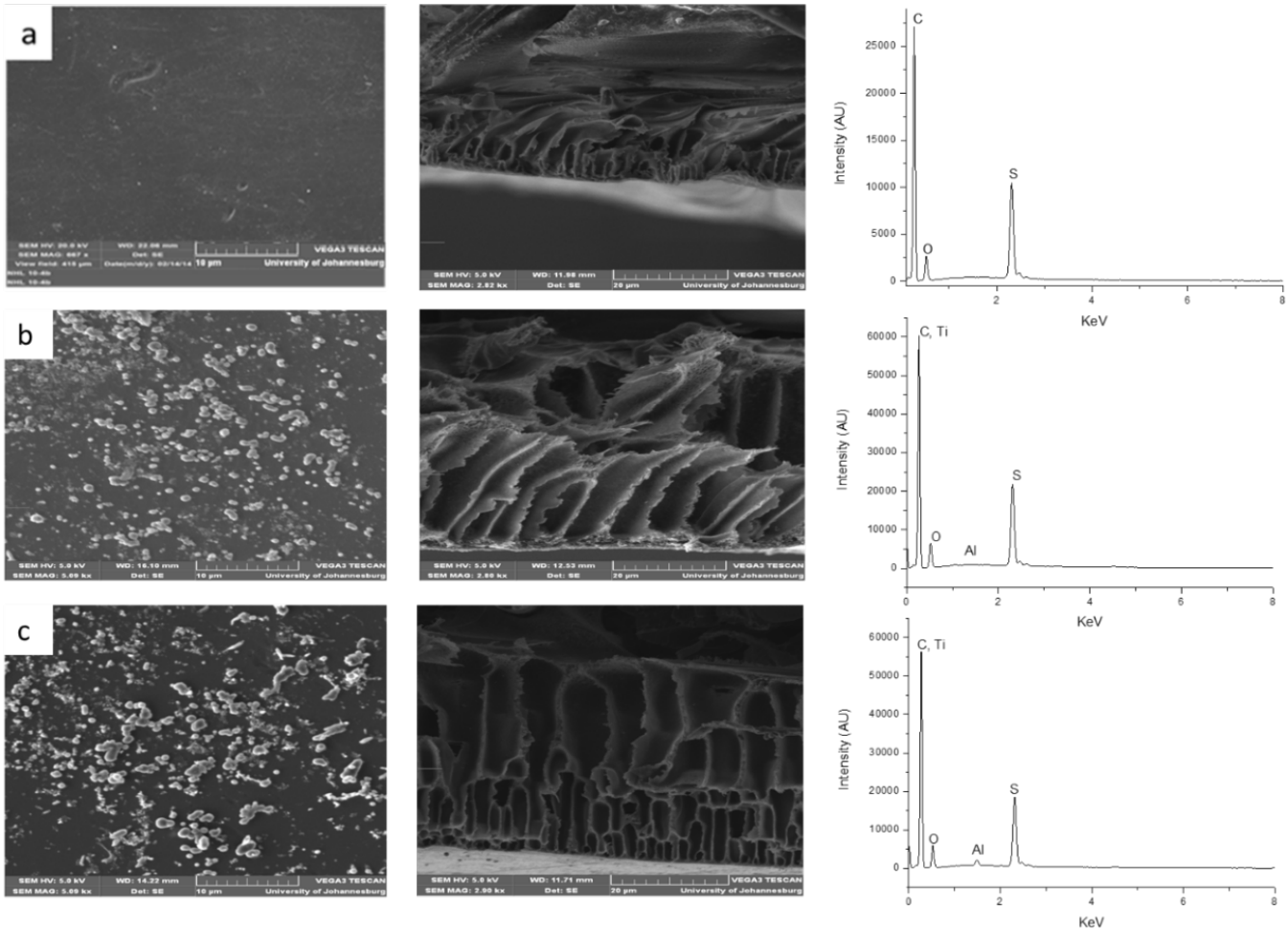

Fig. 3. High resolution scanning electron microscopy images (top-view and cross-section view) and energy dispersive X-ray (EDS) spectra for: (a) pristine membrane; (b) 0.25% PSf/CCA/Ni-TiO_2 membrane; (c) 0.5% PSf/CCA/Ni-TiO_2 membrane.

The structures of the macrovoids of the different membranes seem to have been affected by the introduction of nanoparticles. The 0.25% PSf/CCA/Ni-TiO_2 membrane was found to possess the biggest macrovoids, the size of which is estimated to be ~4.0 µm. On the other hand, macrovoids size of ~2.0 µm was recorded for the 0.50% PSf/CCA/Ni-TiO_2 membrane. With a size of 1.0 µm, macrovoids of the pristine membrane were the smallest. The 0.25% PSf/CCA/Ni-TiO_2 membrane was found to possess uniform macrovoids that were enlarged throughout the cross-section matrix of the membrane. This macrovoid structure may also suggest increased porosity of these membranes. The 0.50% PSf/CCA/Ni-TiO_2 membrane was found to possess macrovoids structures of two types. The macrovoids located towards the surface of the membranes were generally smaller than those at the base of the membranes. Such observations concur with earlier reports which have also suggested that an increase in TiO_2 nanoparticles content in the membrane matrix leads to decreased porosities [30, 35-38]. To this end, a decrease in the size of the macrovoids was observed when the CCA/Ni-TiO_2 content of the PSf/CCA/Ni-TiO_2 membrane was decreased from 0.50% to 0.25%. The effect of nanoparticles on the structure (and by extension the functional properties) of the membranes has also been reported [21]. Such an effect is largely dependent on the order in which the nanoparticles were added during the preparation step rather than the type of the nanoparticles used [21, 34]. This observation can be explained in terms of the viscosity of the dope casting solution, which is known to suppress macrovoid formation [38-40]. Soroko et al. [38] demonstrated that viscosity increases with increased loading of the nanoparticles such as the TiO_2 nanoparticles used in this research study. The direct relationship between viscosity and nanoparticle loading is caused by the adsorption between the exposed –OH functional groups at the surface of TiO_2 nanoparticles as well as the high specific surface area, surface energy and the polymeric chains [36].

3.3.2. Atomic force microscopy studies

The AFM was used as a complimentary tool to the SEM technique in order to gain more insight into the morphological differences of the synthesised membranes (Figure 4). The 0.25% PSf/CCA/Ni-TiO_2 membrane exhibited the most porous surface when compared to the other two membranes. The differences in porosity was confirmed with an SEM investigation (see SEM images in Figure 3). AFM and SEM images show that the 0.25% PSf/CCA/Ni-TiO_2 membrane possess a much more uniform porosity compared to the 0.5% PSf/CCA/Ni-TiO_2 and pristine membranes. The surface of the 0.50% PSf/CCA/Ni-TiO_2 membrane was found to be rougher when compared with the pristine membrane. This was confirmed by the R_a, which was 27.76 nm, 69.17 nm, and 45.05 nm for the pristine membrane, 0.25% PSf/CCA/Ni-TiO_2 and 0.50% PSf/CCA/Ni-TiO_2 membrane, respectively (Table 2). Such an observation is in agreement with the average arithmetic roughness (Ra) values (27.76 nm for the pristine membrane; 69.17 nm for the 0.25% PSf/CCA/Ni-TiO_2 membrane; and 45.05 nm for the 0.50% PSf/CCA/Ni-TiO_2 membrane) listed in Table 2. As also shown in Table 2, the root mean square roughness (R_q) values also followed a similar trend.

Overall, the 0.25% PSf/CCA/Ni-TiO_2 membrane possesses the roughest membrane surface when compared to the other two membranes. Since the modified membranes were found to be rougher than the pristine membrane, it can be concluded that the Ni-TiO_2 nanoparticles are responsible for the increased rough surface and porosity of the membranes. The increased roughness and porosity was confirmed by an SEM/EDS analysis of the membranes (Figure 3). A simple comparative morphological analysis of the 0.25% and 0.50% PSf/CCA/Ni-TiO_2 membranes suggests a direct link between the concentration of the nanoparticles and the morphology of the samples.

Increased macrovoid size, which advances membrane porosity, appears to be aided by lower nanoparticle concentration. Similarly, higher concentrations of the nanoparticles promote the formation of low-sized macrovoids, which in turn lead to smaller pores and a higher compaction of the PSf polymer [38-40]. Results presented in this study have also been corroborated by Zhang et al. [41], who demonstrated increased surface roughness when the nanoparticle dosage of the UF membranes modified with TiO_2 nanoparticles was increased.

The height distribution (H_d) of the membranes also varied with the concentration of the membrane nanoparticles (see Figure 4 and Table 2). Although the H_d of the 0.50% PSf/CCA/Ni-TiO_2 membrane was found to be the highest (420-700 nm), the normal curve distribution of the H_d graph was smaller than that of the 0.25% PSf/CCA/Ni-TiO_2 membrane. Furthermore, given the lower peak density associated with the 0.50% PSf/CCA/Ni-TiO_2 membrane, an indirect relationship between the surface area and nanoparticle concentration of the PSf/CCA/Ni-TiO_2 membrane can be inferred (Table 2). The relationship inferred was that the higher the concentration, the lower the surface area available for adsorption of water molecules, because of the already attached nanoparticles.

3.4. Water permeability, hydrophilicity and water uptake analysis of membranes

The effect of the CCA/Ni-TiO_2 nanoparticles on the water permeability, hydrophilicity and water uptake of the membranes was investigated. The pristine membrane was found to have a permeate flux of between 130.95±4.50 $L.m^{-2}.h^{-1}$ and 232.14±3.45 $L.m^{-2}.h^{-1}$ at applied pressures of 13.8 bar and 27.6 bar, respectively. The permeate flux of 0.25% and 0.50% PSf/CCA/Ni-TiO_2 membranes and ranged between 213.50±6.40 $L.m^{-2}.h^{-1}$ – 296.70±4.75 $L.m^{-2}.h^{-1}$ and 105.18±4.52 $L.m^{-2}.h^{-1}$ – 157.74±5.67 $L.m^{-2}.h^{-1}$, respectively at the same pressures mentioned above (Figure 5). It is noteworthy that the 0.25% PSf/CCA/Ni-TiO_2 membrane was found to possess the highest pure water flux at all the pressures (13.8 bar, 20.7 bar, 27.6 bar) investigated; this was followed by the pristine membrane, with the 0.50% PSf/CCA/Ni-TiO_2 membrane being the lowest.

Moustakes et al. [5] has indicated that membranes modified with TiO_2 nanoparticles have extremely high flux properties. The water permeability of the modified membranes was almost one order of magnitude higher than that of the unmodified γ-alumina membranes. This could be related to the higher water permeability of the membranes modified with 0.25% CCA/Ni-TiO_2 nanoparticles. In accordance with findings by Rahimpour et al. [42], which showed a decrease in water permeability when the TiO_2 nanoparticles weight percentage was increased, the membranes modified with CCA/Ni-TiO_2 nanoparticles showed a slight decrease in water permeability when the concentration was increased from 0.25 to 0.50%.

These observations can be explained by considering the morphological structure of the membranes. The cross-section observations of the SEM images and AFM images indicated that the 0.25% PSf/CCA/Ni-TiO_2 membrane was more porous than the other two membranes. Therefore, higher porosity results in higher flux in the membranes. The increased peak densities and roughness of these membranes also contribute to the increased surface area, which translated into increased water permeability (Table 2). Previous studies indicate a direct relationship between the surface roughness and the surface area of the membrane [36, 43]. In practical terms, it suffices to say that increased surface area of the membrane leads to increased contact of the membrane with water molecules, which in turn leads to increased water permeability [36, 43].

Table 2
Peak to peak maximum distance (Sy), height distribution (Hd), average arithmetic roughness (Ra), root mean square roughness (Rq), and peak densities (Pn) obtained from AFM analysis (image scan area; 30 µm X 30 µm).

Membrane	R_q (nm)	R_a (nm)	S_y (nm)	H_d (nm)	P_n
Pristine Membrane	35.47	27.76	5.38	0.00 - 330	149
0.25% PSf/CCA/Ni-TiO_2	89.14	69.17	4.36	140 - 560	157
0.50% PSf/CCA/Ni-TiO_2	72.78	45.05	28.42	420 - 700	121

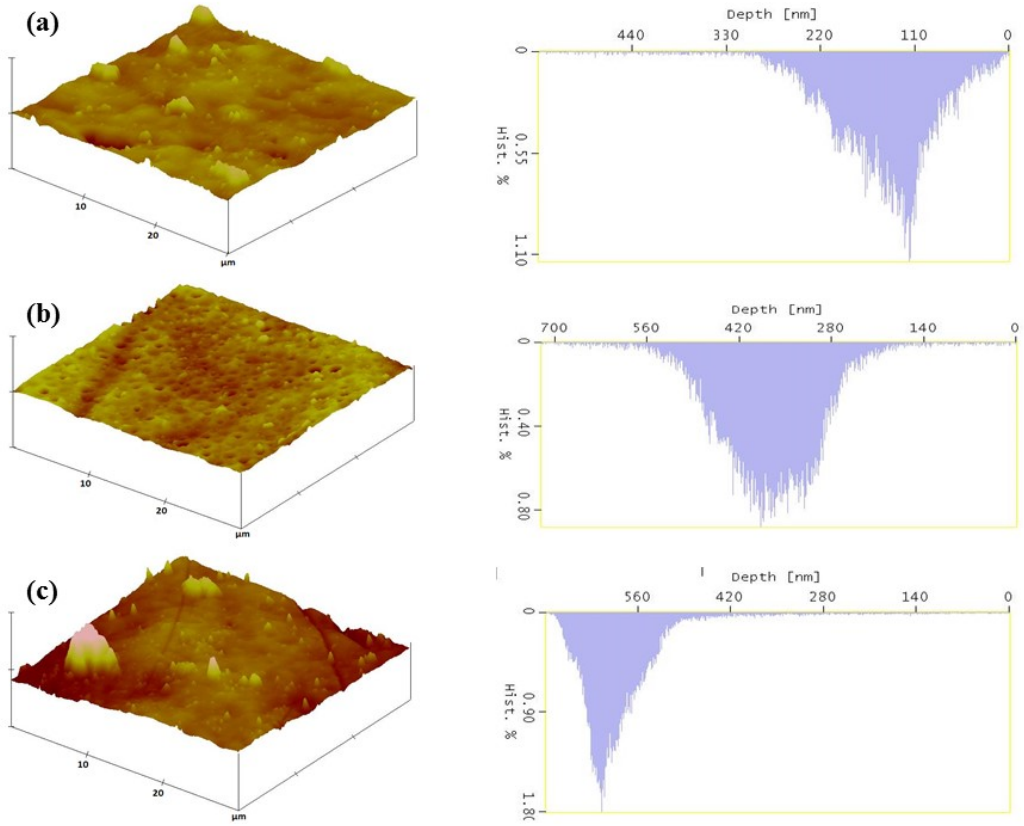

Fig. 4. AFM images and peak height histogram of the image frame 30 µm x 30 µm: (a) pristine membrane; (b) 0.25% PSf/CCA/Ni-TiO_2 membrane; (c) 0.50% PSf/CCA/Ni-TiO_2 membrane.

Table 3
Contact angle, water uptake and permeation values for membranes

Membrane	Contact Angles (º)	Water Uptake (%)	Permeation (L. m^{-2}. h^{-1}. bar^{-1})
Pristine Membrane	70.30±2.24	17.65±0.30	8.90±1.20
0.25% PSf/CCA/Ni-TiO_2	71.57±1.50	13.30±1.34	12.7±0.70
0.50% PSf/CCA/Ni-TiO_2	72.23±1.80	32.00±0.50	6.37±1.80

The contact angle (CA) measurements of the membranes were studied using deionised water in an OCA Dataphysics Contact Angle instrument. The pristine membrane had a CA value of 70.30±2.24º (see Table 3), which corresponds with the reported literature value [44]. However, the 0.25% PSf/CCA/Ni-TiO_2 membrane and 0.50% PSf/CCA/Ni-TiO_2 membrane had contact angles at 71.57±1.50º and 72.23±1.80º, respectively (Table 3). The CA values of 71.57±1.50º and 72.23±1.80º for the 0.25% and 0.50 PSf/CCA/Ni-TiO_2 membranes concur with similar CA values reported for polyvinylidene difluoride (PVDF) UF membranes modified with TiO_2 nanoparticles, which ranged between 70.00º and 74.00º [41]. The increased roughness of the modified membranes was shown to affect the hydrophilicity of the modified membranes, by making it less hydrophilic as demonstrated in Tables 2 and 3.

A comparative analysis of the CA measurements of the modified and pristine membranes revealed a slight increase in the CA measurement of the modified membranes upon the introduction of the nanoparticle component. While the incorporation of TiO_2 nanophotocatalysts onto UF PSf membranes is known to decrease the CA measurements of modified membranes [44-46], such a decrease in the CA was not observed. In contrast, only a slight increase in the CA of the modified membranes was observed. This slight increase in the CA is attributable to an increase in the roughness of the modified membranes [41]. Furthermore, the increase in the CA can be accounted for by considering the hydrophobic carbon coated alumina support on which the TiO_2 nanoparticles were supported. The interaction between the carbon-coated-alumina and the polysulfone could lead to decreased hydrophilicity. In other words, in this case, an increase in the membrane surface area could potentially lead to a slight decrease in the hydrophilicity of the modified membranes.

Water uptake in PSf UF membranes is determined by the adsorption of water molecules on the surface of the membrane. Such an adsorption enables preferential diffusion of water molecules through the membrane matrix [47, 48]. The disadvantages of excessive water uptake within hydrophilic membranes include pore shrinkage and membrane breakage, resulting in poor membrane performance [49-51]. Therefore, highly swollen membranes are not suitable as membrane materials, even with high water affinity [48].

The water uptake performance of the modified and unmodified membranes was studied. While the pristine membrane was found to possess a water uptake of 17.65±0.30%, it was established that the water uptake of the 0.25% and 0.05 PSf/CCA/Ni-TiO_2 membranes were 13.30±1.34% and 32.00±0.50%, respectively (see Table 3). Compared to the other membranes, the water uptake of the 0.50% PSf/CCA/Ni-TiO_2 membrane was the highest. These results indicate no correlation could be established between the water uptake and permeability in these membranes.

3.5. Electrostatic interactions of membranes with NaCl ions

The membranes were tested for NaCl salt rejection at a concentration of 2.00 g/L and pressures of 13.8, 20.7 and 27.6 bars [6]. Figure 6 shows a comparison of the NaCl salt rejection with its salt water permeability. Generally, a water permeate flux drop was noted when the salt water permeability (Figure 6) was compared with the pure water flux (Figure 5). At a bar pressure of 13.8 and 27.6, the water permeate flux of the pristine membrane salt ranged from 110.04±2.89 $L.m^{-2}.h^{-1}$ and 180.45±2.56 $L.m^{-2}.h^{-1}$ while the pure water flux was recorded at 130.95±4.50 $L.m^{-2}.h^{-1}$ to 232.14±3.45 $L.m^{-2}.h^{-1}$. A similar pattern was observed for the modified membranes. The lower salt water flux (i.e. relative to the pure water flux), which resulted was due to the existence of competition between water molecules and the dissolved salt for the same porous pathways. Hence, the decrease in salt water permeate flux. Furthermore, the general trend that was also observed is that, increasing the pressure increase water permeability and decreased NaCl salt rejection as shown in Figure 6. As a second general trend, an increase in the pressure increased the water permeability, which ultimately led to a decrease in the NaCl salt rejection (see Figure 6).

Ultrafiltration membranes have relatively large surface pores and high water permeability and their operation requires low energy consumption [50]. Besides photocatalysis, the CCA/Ni-TiO_2 nanoparticles are expected to reduce scaling on the membrane surface because of the presence of –OH groups in the TiO_2 nanoparticles, which have been shown in other research studies to reduce membrane fouling [50-54]. Although UF membranes are generally viewed as a size-based separation technique, it has been shown that particle and membrane charge also influences the rejection of dissolved salts [51-55]. In this research study, the NaCl salt (2.00 g/L) was selected as model salt for investigation because of its very small size that enables it to easily pass through the UF membrane pores on the basis of the size-exclusion principle [56]. This suggests that an increase in the NaCl salt rejection by the membranes may not be due to the size-exclusion but a result of the electrostatic interactions between the solute and the UF membrane surface [57-59].

In this study, the rejection of the NaCl salt by the 0.25% and 0.50% PSf/CCA/Ni-TiO_2 membranes at 13.8 bar was recorded at 31.38±1.23% and 31.59±1.12%, respectively (Figure 5). These NaCl salt rejection values were found to be higher than that of the pristine membrane, which was 12.76±1.10% at the same pressure. Generally, the modification of the membranes showed increased rejection capacity compared to the unmodified membrane. This clearly suggests that the electrostatic interactions played a much more prominent role in the rejection of the modified membranes compared to the size exclusion principle [51, 57-63]. This could be due to the presence of –OH functional groups emanating from the TiO_2 nanoparticles [63]. The –OH functional groups of the TiO_2 nanoparticles have been shown to be electrostatic at pH 7.00, the pH level at which our experiments were carried out. Furthermore, the NaCl salt gets ionised at the same pH level and thus exist as Na^+ cation and Cl^- anions. Polysulfone UF membranes were reported to be capable of rejecting anionic arsenate [58, 59]. The rejection of ionic salts is dependent on the pH of the solutions and this can be explained by Donnan exclusion and formation of an electrical double layer in the membrane pores [61, 64]. Labbez et al. explained that the greater the ion rejection due to electrostatic repulsion may result in a stronger overlapping of the electrical double layers in the pores [64].

3.6. Rejection of Cr^{3+} heavy metal ions

The membranes were also tested for their Cr^{3+} heavy metal rejection capacity from dye wastewater. The unmodified membranes showed a Cr^{3+} rejection of 28.32±1.65%, 26.67±1.87% and 17.60±2.00% at 13.8, 20.7 and 27.6 pressure bar, respectively (Figure 7a). This indicates that an increase in the pressure leads to a decrease in the rejection capacity of the membranes In comparison to that of the 0.25% PSf/CCA/Ni-TiO_2 UF membranes, the Cr^{3+} rejection capacity was higher than that of the unmodified membranes. The Cr^{3+} rejection for these modified membranes was found to range between 56.28±2.54% and 66.12±1.76%. Moreover, the rejection of the pollutant by these modified membranes was found to increase with increasing pressure. For example, the rejection of the Cr^{3+} was found to be 56.27±2.54%, 65.29±1.90%, and 66.12±1.76%, at pressures of 13.8, 20.7 and 27.6 bars, respectively (Figure 7b). This increase in the rejection capacity is ascribed to the Ni-TiO_2 nanoparticles that increases the electrostatic repulsion of the modified membranes.

The membranes modified with 0.50% CCA/NiTiO_2 nanoparticles were also found to possess a higher reject capacity for Cr^{3+} heavy metals when compared with the unmodified membranes. The rejection capacity was found to be 60.48±1.52%, 62.62±2.91%, and 57.25±1.99% at the same respective pressures mentioned above. Generally, a significant decrease in the rejection capacity was noted when the pressure was increased for the unmodified membranes. However, for the modified membranes, a steady but slight rejection capacity pattern was observed for the 0.25% CCA/Ni-TiO_2 membranes. Bet-Moushoul et al. [65] attributed the enhancement in rejection capacity to the –OH groups of the TiO_2 nanoparticles. These –OH groups created an extra uniform settlement and more accumulation of the TiO_2 nanoparticles on the membrane surface. As a result, the TiO_2 nanoparticles established co-ordinate covalent bonds with the –OH groups on the surface of the membranes [65, 66].

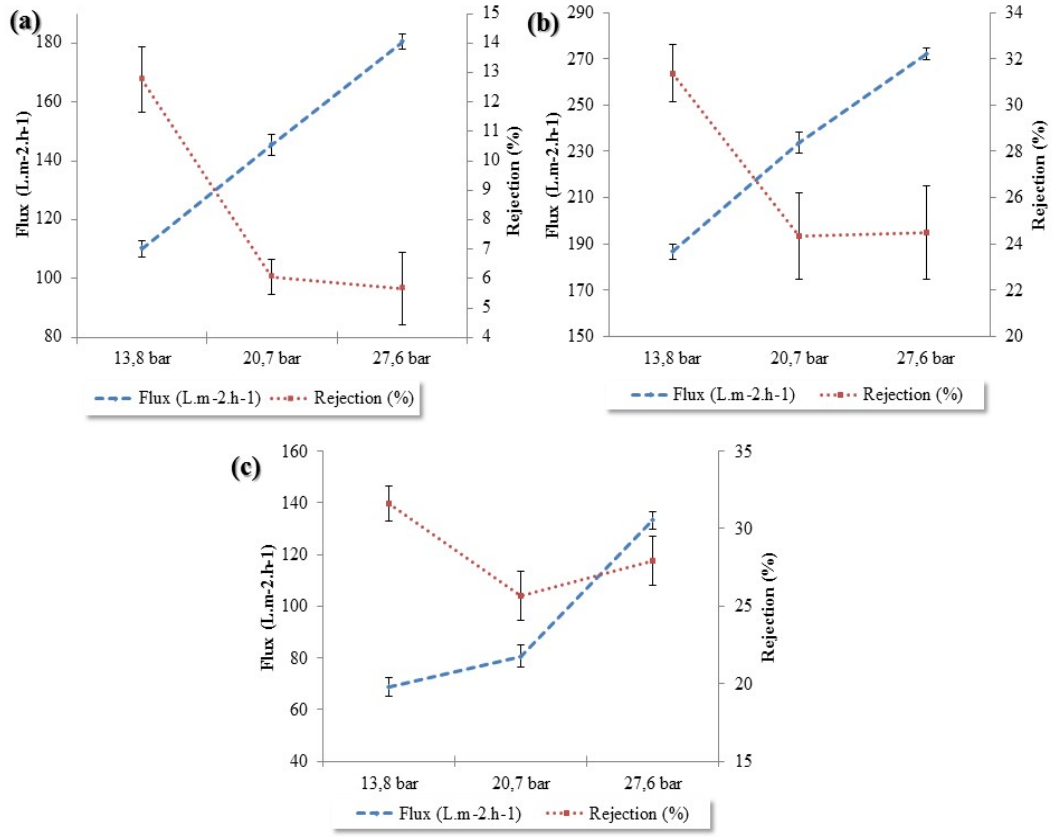

Fig. 6. NaCl salt (2.00 g/L) rejection of the membranes under different pressures: (a) pristine membrane; (b) 0.25% PSf/CCA/Ni-TiO_2 membrane; (c) 0.5% PSf/CCA/Ni-TiO_2 membrane.

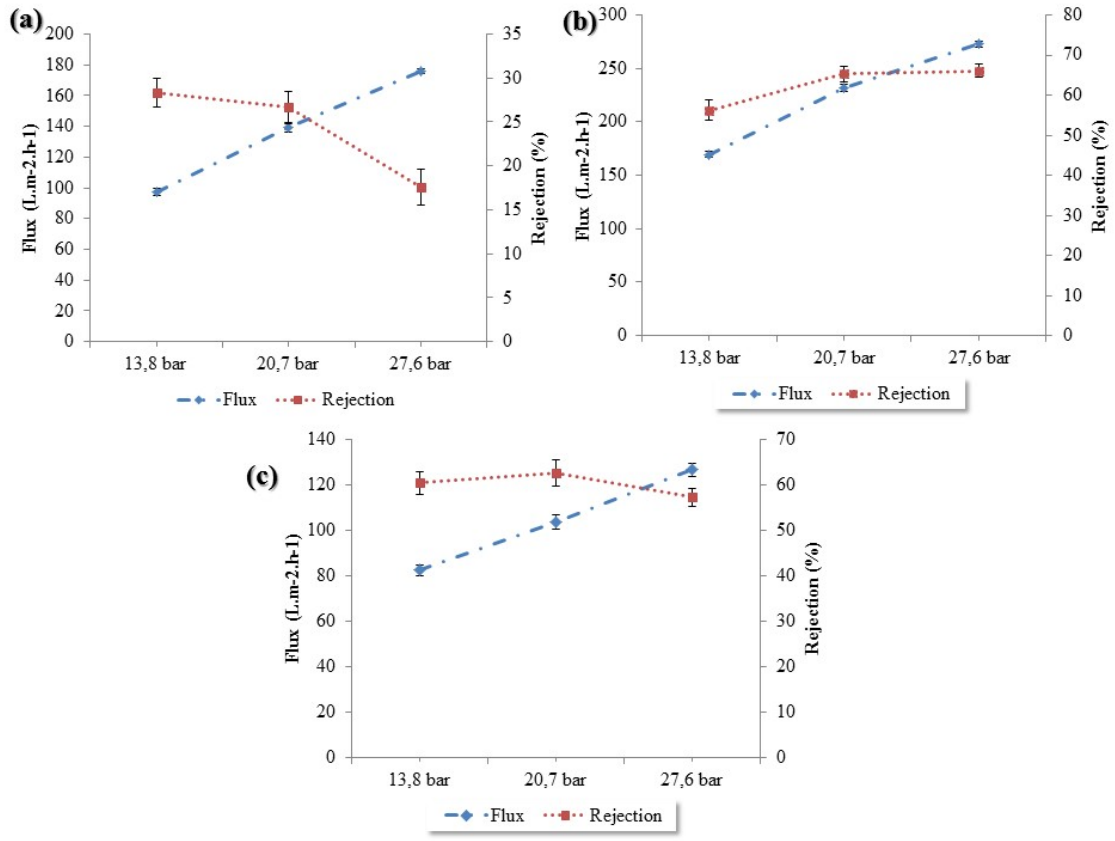

Fig. 7. Cr^{3+} (2.00 g/L) rejection of the membranes under different pressures: (a) unmodified membrane; (b) 0.25% PSf/CCA/Ni-TiO_2 membrane; (c) 0.5% PSf/CCA/Ni-TiO_2 membrane.

3.7. Photodegradation studies

3.7.1. Visible light photodegradation of methyl orange and bromophenol blue

The photodegradation of methyl orange and bromophenol blue (10 mg.L^{-1}) by 0.25% and 0.50% PSf/CCA/Ni-TiO_2 membranes was studied under visible light illumination as shown in Figure 7. The methyl orange (monitored at 470 nm) and brophenol blue (monitored at 580 nm) dyes in the visible spectrum were found to have a photolysis (without a catalyst) of 2.10% (0.21 mg.L^{-1}) and 2.30% (0.23 mg.L^{-1}), respectively. According to Figure 7, the 0.25% PSf/CCA/Ni-TiO_2 membrane demonstrated lower degradation capacity towards the methyl orange (50.5%; 5.05 mg.L^{-1}) compared to the bromophenol blue (70.0%; 3.01 mg.L^{-1}) after 180 minutes. On the other hand, only 36.5% (6.36 mg.L^{-1}) of the methyl orange was degraded after 180 minutes when the 0.50% PSf/CCA/Ni-TiO_2 membrane was used. It is evident from these results that the 0.25% PSf/CCA/Ni-TiO_2 membrane is much more effective in the degradation of the methyl orange dye when compared with the 0.50% PSf/CCA/Ni-TiO_2 membrane (Figure 8).

As illustrated in Figure 8, an initial high degradation rate associated with both 0.25% and 0.50% PSf/CCA/Ni-TiO_2 membranes was recorded when bromophenol blue was used as a model dye pollutant. However, the rate of photodegradation seems to recede after 30 minutes. At the end of the 180 minute period of investigation, 70.0% of the bromophenol blue was found to have been degraded by the 0.25% PSf/CCA/Ni-TiO_2 membrane compared to the 81.0% bromophenol blue degradation achieved using the 0.50% PSf/CCA/Ni-TiO_2 membrane. Generally, a higher degradation rate by the photocatalytic membranes was observed for the bromophenol blue when compared with the methyl orange dye.

The degradation rate of the methyl orange was also lower than the rate that was observed for Rhodamine B using the same nanophotocatalysts with a support system. However, the bromophenol blue degradation rate was either similar or higher than when an unsupported CCA/Ni-TiO_2 nanophotocatalysts was used. Although nanoparticles supported on polymeric membranes present the challenge of the inaccessibility of the nanoparticles as they get embedded in the membrane matrix, these membranes performed fairly well compared to the unsupported nanophotocatalysts. Not only was it evident that the embedding of nanophotocatalysts on PSf UF membranes provides support, it also did not significantly reduce the capability of the nanophotocatalyst to degrade dye pollutants.

The PSf/CCA/Ni-TiO_2 nanophotocatalytic membranes (1:1 ratio) were previously used by Mahlambi et al. for the degradation of Rhodamine B under visible light irradiation and a degradation efficiency of 98.0% was achieved [27, 28]. In this study, a lower Rhodamine B degradation efficiency of 71.5% was achieved within 180 minutes when the PSf/CCA/Ni-TiO_2 nanophotocatalytic membranes were used as catalytic membranes. The slight decrease in the degradation efficiency can be attributed to the decreased accessibility of the nanophotocatalysts that are embedded in the polysulfone polymer matrix. On the other hand, the PSf/CCA/Ni-TiO_2 were found to be more photoactive towards bromophenol blue compared to methyl orange. For example, while up to 70.0% and 81.0% of the bromophenol blue was degraded by 0.25 and 0.50% PSf/CCA/Ni-TiO_2 membranes, respectively, only 36.5% and 50.5% methyl orange degradation efficiency was achieved within the same time frame (i.e. 180 minutes) when the same membranes were employed. Therefore, the degradation efficiency was decreased when compared to when the unsupported nanophotocatalysts are suspended in the dye solution.

It has been well established that the available surface of the TiO_2 nanoparticles plays a vital role in the reaction pathway for the degradation of organic pollutants. For this reason, successful photodegradation has been largely achieved with nanocatalysts that have not been supported on polymeric membranes. However, such an approach is accompanied by post-treatment challenges. The nanocatalysts would often need to be separated from the wastewater immediately after treatment and a solid-liquid separation step is therefore required. As a result, the additional separation step renders this approach more expensive and impossible to apply at large scale.

It is however noteworthy that while the immobilization of the catalysts in this study decreased the surface area, high photodegradation efficiencies were nevertheless achieved. Similar results have been reported in several studies. For example, 100% methylene blue degradation using PVDF/TiO_2 ultrafiltration membranes has been achieved [65, 67]. Albeit at a lower degradation efficiency rate of 11.0%, the degradation of 2-chloroethylphenyl sulphide by PANI-PEO/TiO_2 composites has been reported [68]. In another study, 77.20% of methyl orange degradation using PVDF/TiO_2/AO membranes has been achieved [69]. It has also been shown that PVDF/TiO_2 membranes can degrade brilliant green and indigo carmin at a respective rate of 2.4 mmol L^{-1} min^{-1} and 6.1 mmol L^{-1} min^{-1} [70]. Therefore, immobilization of nanophotocatalysts on membranes can potentially provide support without any significant loss of the photodegradation capability of the membranes.

3.7.2. Photodegradation Kinetic Studies

The kinetic models revealed that both the photodegradation of methyl orange and bromophenol blue followed a pseudo first order reaction rate (Figure 9). The apparent constants were found to be 0.7032 min^{-1} and 0.4541 min^{-1} for the photodegradation of methyl orange by 0.25% and 0.50% PSf/CCA/Ni-TiO_2 membranes, respectively. For the degradation of bromophenol blue, the apparent rate constants were 1.204 min^{-1} and 1.661 min^{-1} for 0.25% and 0.50% PSf/CCA/Ni-TiO_2 membranes, respectively.

On the basis of photodegradation kinetic results, it was established that the polymeric membranes displayed decreased photodegradation efficiencies. Although embedding the titania nanoparticles onto the CCA supports only reduced the problems associated with agglomeration, however it could not deal with post water treatment due to its powdery nature of the CCA/Ni-TiO_2 nanoparticles. The benefits associated with ease of use of the membranes, these modified PSf/CCA/Ni-TiO_2 membranes far outweighs the slight decrease in photocatalytic efficiency associated with using the modified membranes.

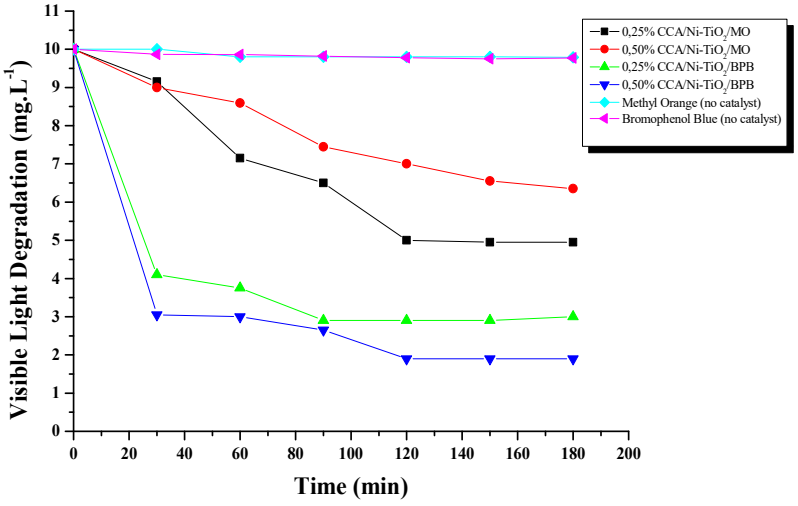

Fig. 8. Visible light degradation of methyl orange (MO) and bromophenol blue (BPB) using 0.25% and 0.5% PSf/CCA/Ni-TiO_2 membranes.

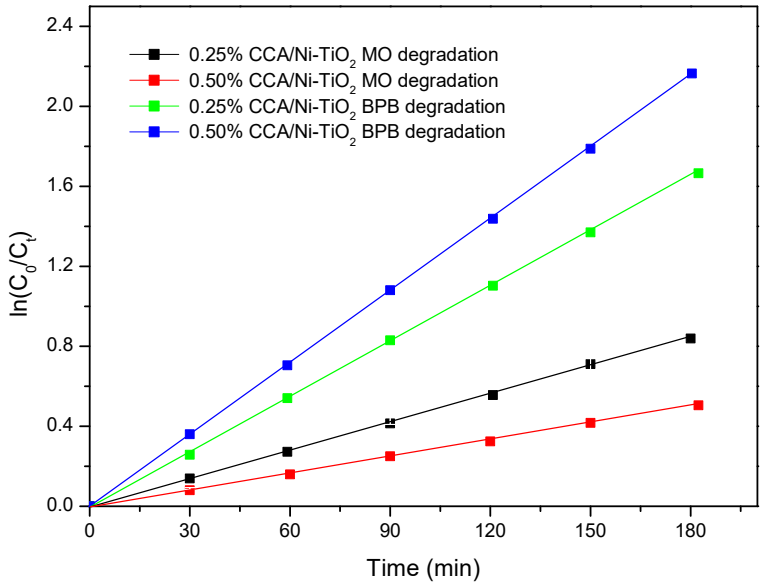

Fig. 9. Linear transform of visible light degradation of methyl orange and bromophenol blue by PSf/CCA/Ni-TiO_2 embedded polysulphone membranes.

4. Conclusions

The CCA/Ni-TiO_2 nanoparticles were successfully incorporated into PSf membranes. Such an incorporation was confirmed by results from SEM, EDS, RAMAN, FTIR and AFM analyses. The effect of nanoparticle loading on membrane structure and performance was studied. Using criteria such as flux and rejection capacity measurements and membrane structural indicators (i.e. nanoparticle agglomeration, membrane porosity and water uptake studies measurements), it was demonstrated that the membrane performance for the 0.25wt% membrane loading was the better than that of the 0.5wt% loading. The bromophenol blue model pollutant was more easily degraded by the membranes compared to the methyl orange. Overall, the successful synthesis and application of the UF membranes was carried out. Therefore, significant strides were made in the fabrication of nanoparticle-embedded membranes for application in water treatment.

Acknowledgements

The authors would like to acknowledge the Department of Applied Chemistry at the University of Johannesburg and the Department of Science and Technology/Mintek Nanotechnology Innovation Centre (South Africa) for funding this work and providing the requisite technical assistance and infrastructure.

References

[1] L. Bian, Y.-j. Li, J. Li, J.-n. Nie, F.-q. Dong, M.-x. Song, L.-s. Wang, H.-l. Dong, H.-l. Li, X.-q.X.-q. Nio, X.-y. Zhang, X.-x. Li, L. Xie, Photovoltage response of (XZn) $Fe_2O_4BiFeO_3$ (X=Mg, Mn, or Ni) interface for highly selective Cr^{3+}, Cd^{2+}, Co^{2+} and Pb^{2+} ions detection. J. Hazard Mater. 336 (2017) 174-187.

[2] T. Sharif, A. Niaz, M. Najeeb, M.I. Zaman, M. Ihsan, M. Sirajuddin, Isonicotini cid hydrazide-based silver nanoparticles as simple calorimetric sensor for the detection of Cr^{3+}. Sens. Actuators. B .Chem. 216 (2015) 402-408.

[3] A.O. Lukina, C. Boutin, O. Rowland, D.J. Carpenter, Evaluating trivalent chromium toxicity on wild terrestrial and wetland plants. Chemosphere. 162 (2016) 355-366.

[4] T.M. Zewail, N.S. Yousef, Chromium ions (Cr^{6+} and Cr^{3+}) removal from synthetic wastewater by electrocoagulation using vertical expanded Fe anode. J. Electroanal. Chem. 735 (2014) 123-128.

[5] N.G. Moustakes, F.K. Katsaros, A.G. Kontos, G.Em. Ramanos, D.D. Dionysiou, P. Falaras, Visible light active TiO2 photocatalytic filtration membranes with improved permeability and low energy consumption. Catalysis Today 224 (2014) 56-69.

[6] F.Q. Mir, A. Shukla, Negative rejection of NaCl in ultrafiltration of aqueous solution of NaCl and KCl using solidate octahydrate zeolite-clay charged ultrafiltration membrane. Ind. Eng. Chem. Res. 49 (2010) 6539-6546.

[7] S. Darvishmanesh, X. Qian, S.R. Wickramasingh, Responsive membranes for advanced separations, Curr. Opin. Chem. Eng. 8 (2015) 98-104.

[8] J. Vanneste, W.J. Peumans, E.J.M. Van Damme, S. Darvishmanesh, K. Bernaerts, J.M.C. Geuns, B. Van der Bruggen, Novel natural and biomimetic ligands to enhance selectivity of membrane processes for solute–solute separations: beyond nature's logistic legacy. J. Chem. Techn. Biotech. 89 (2014) 354-371

[9] .A.Razmjou, E. Arifin, G. Dong, J. Mansouri, V. Chen, Superhydrophobic modification of TiO2 nanocomposite PVDF membranes for applications in membrane distillation. *J. Membr. Sci.* 415–416 (2012) 850-863.

[10] L. Bazinet, J.-F. Poulin, J. Amiot, Effect of conditioning ultrafiltration membranes on their performances in electrodialysis with ultrafiltration membrane. Sep. Sci. Technol. 42 (2007) 2501 - 2518.

[11] Y. Mansourpanah, E. Momeni-Habili, Investigation the separation properties of TiO_2-TFC nanocomposite membranes by comparing the presence or absence of UV irradiation; membrane preparation and characterization. J. Membr. Sci. Res. 1 (2015) 26-33.

[12] M. Ulbright, Advanced Functional Polymer Membranes. Polym. 47 (2006) 2217-2262.

[13] T. Wang, Y. Yang, J. Zheng, Q. Zhang, S. Zhang, A novel highly permeable positively charged nanofiltration membranes based on a nanoporous hyper-crosslinked polyamide barrier layer. J. Membr. Sci. 448 (2013) 180-189.

[14] M.S. Jyothi, V. Nayak, M. Padaki, R.G. Balakrishna, K. Soontarapa, Aminated polysulfone/TiO_2 composite membranes for an effective removal of Cr(VI). Chem. Eng. J. 283 (2016) 1494-1505.

[15] V. Buscio, M. Crespi, C. Gutiérrez-Bouzán, Application of PVDF ultrafiltration membranes to treat and reuse textile wastewater. Desalin. Water Treat. 57 (2016) 8090-8096.

[16] G. Arthanareeswaran, D. Mohan, M. Raajenthiren, Preparation and performance of polysulfone-sulfonated poly (ether ether ketone) blend ultrafiltration membranes. Part I. Appl. Surf. Sci. 253 (2007) 8705-8712.

[17] B.-G. Wang, M. Ando, H. Yin, B. Hong, Y. Peng, Mathematical modelling of flux in ultrafiltration membrane for water treatment. Sep. Sci. Technol. 41 (2006) 1179-1191.

[18] D.Y. Koseoglu-Imer, B. Kose, M. Altinbas, I. Koyuncu, The production of polysulfone (PS) membrane with silver nanoparticles (AgNP): Physical properties, filtration performances, and biofouling resistances of membranes. J. Membr. Sci. 428 (2013) 620-628.

[19] E. Bet-Moushoul, Y. Mansourpanah, Kh Farhadi, M. Tabatabaei, TiO_2 nanocomposite based polymeric membranes: A review on performance improvement for various applications in chemical engineering processes. Chem. Eng. J. 283 (2016) 29-46.

[20] F. Fayyazi, E.A. Fajani, H. Mahdavi, Chemically modified polysulfone membrane containing Pd nanoparticles: Preparation, characterization and application as an efficient catalytic membrane for Suzuki reaction. Chem. Eng. Sci. 134 (2015) 549-554.

[21] M. Homayoonfal, M.R Mehrnia, M. Shariaty_Niassar, A. Akbari, A.F. Ismail, T.A. Matsuura, A comparison between blending and surface deposition methods for the preparation of iron oxide/polysulfone nanocomposite membranes. Desalination 354 (2014) 125-142.

[22] S.P. Malinga, O.A. Arotiba, R.W.M. Krause, S.F. Mapolie, M.S. Diallo, B.B. Mamba, Cyclodextrin-dendrimer functionalized polysulfone membrane for the removal of humic acid in water. J. Appl.Polym. Sci. 130 (2013) 4428-4439

[23] Y. Mansourpanah, S.S. Madaeni, A. Rahimpour, A. Farhadian, A.H. Taheri, Formation of appropriate sites on nanofiltration membrane surface for binding TiO_2 photo-catalyst: performance, characterization and fouling resistant capability. J. Membr. Sci. 330 (2009) 297-306.

[24] Q. Wang, X. Wang, Z. Wang, J. Huang, Y. Wang, PVDF membranes with simultaneously enhanced permeability and selectivity by breaking the trade-off effect *via* atomic layer deposition of TiO_2. J. Membr. Sci. 442 (2013) 57-64.

[25] J. Méricq, J. Mendret, S. Brosillon, C. Faur, High performance PVDF-TiO_2 membranes for water treatment. Chem. Eng. Sci. 123 (2015) 283-291.

[26] A. Rahimpour, M. Jahanshahi, B. Rajaeian, M. Rahimnejad, TiO_2 entrapped nano-composite PVDF/SPES membranes: preparation, characterization, antifouling and antibacterial properties. Desalination 278 (2011) 343-353.

[27] A.D. Kiadehi, M. Jahanshahi, A. Rahimpour, A.A. Ghoreyshi, Fabrication and evaluation of functionalized nano-titanium dioxide (F-nanoTiO2)/polysulfone (PSf) nanocomposite membranes for gas separation. Iranian J. Chem. Eng. 11 (2014) 40-49.

[28] M.M. Mahlambi, A.K. Mishra, S.B. Mishra, R.W. Krause, B.B. Mamba, A.M. Raichur, Effects of metal ions (Ag, Co, Ni, Pd) on the visible light degradation of Rhodamine B by carbon-covered-alumina-supported TiO_2 in aqueous solutions. Ind. Eng. Chem. Res. 52 (2013) 1783-1794.

[29] M.M. Mahlambi, A.K. Mishra, S.B. Mishra, A.M. Raichur, B.B. Mamba, R.W. Krause, Layer-by-layer self-assembled metal-ion (Ag-, Co-, Ni-, and Pd-) doped TiO2 nanoparticles: Synthesis, characterization, and visible light degradation of Rhodamine B. J. Nanomat. 2012 (2012) 1-12.

[30] C.P. Leo, W.P. Cathie Lee, A.L. Ahmad, A.W. Mohammad, Polysulfone membranes blended with ZnO nanoparticles for reducing fouling by oleic acid. Sep. Purif. Technol. 89 (2012) 51-56.

[31] S. Balta, A. Sotto, P. Luis, L. Benea, B. van der Bruggen, J. Kim, A new outlook on membrane enhancement with nanoparticles: The alternative of ZnO. J. Membr. Sci. 389 (2012) 155-161.

[32] Y. Yang, H. Zhang, P. Wang, Q. Zheng, J. Li, The influence of nano-sized TiO_2 fillers on the morphologies and properties of PSF UF membrane. J. Membr. Sci. 288 (2007) 231-238.

[33] H.B. Park, J. Kamcev, L.M. Robson, M. Elimelech, R.D. B.D. Freeman, Maximizing the right stuff: The trade-off between membrane permeability and selectivity. Science 356 (2017) DOI:10.1126/science.aab0530.

[34] J. Kim, B. van der Bruggen, The use of nanoparticles in polymeric and ceramic membrane structures: review of manufacturing procedures and performance improvement for water treatment. Environ. Pollut. 158 (2010) 2335-2349.

[35] Y. Devrim, S. Erkan, N. Baç, I. Eroğlu, Preparation and characterization of sulfonated polysulfone/titanium dioxide composite membranes for proton exchange membrane fuel cells. Int. J. Hydrogen Energy 34 (2009) 3467-3475.

[36] L.Y. Ng, A.W. Mohammad, C.P. Leo, N. Hilal, Polymeric membranes incorporated with metal/metal oxide nanoparticles: A comprehensive review. Desalination 308 (2013) 15-33.

[37] P. Pandey, R.S. Chauhan, Membranes for gas separation. Prog. Polym. Sci. 26 (2001) 853-893.

[38] I. Soroko, A. Livingston, Impact of TiO_2 nanoparticles on morphology and performance of crosslinked polyimide organic solvent nanofiltration (OSN) membranes. J. Membr. Sci. 343 (2009) 189-198.

[39] Y. Orooji, M. Faghih, A. Razmjou, J. Hou, P. Moazzam, N. Emami, M. Aghababaie, F. Nourisfa, V. Chen, W. Jin, Nanostructured mesoporous carbon polyethersulfone composite ultrafiltration membrane with significant low protein adsorption and bacterial adhesion. Carbon. 111 (2017) 689-704.

[40] N. Peng, T.-S. Chung, K.Y. Wang, Macrovoid evolution and critical factors to form macrovoid-free hollow fiber membranes. J. Membr. Sci. 318 (2008) 363-372.

[41] J. Zhang, Z. Wang, X. Zhang, X. Zheng, Z. Wu, Enhanced antifouling behaviours of polyvinylidene fluoride membrane modified through blending with nano-TiO_2/Polyethylene glycol mixture. Appl. Surf. Sci. 345 (2015) 418–427.

[42] A. Rahimpour, S.S. Madaeni, A.H. Taheri, Y. Mansourpanah, Coupling TiO_2 nanoparticles with UV irradiation for modification of polyethersulfone ultrafiltration membranes. J. Membr. Sci. 313 (2008) 158-169.

[43] S.Y. Kwak, S.G. Jung, S.H. Kim, Structure-motion-performance relationship of flux-enhanced reverse osmosis (RO) membranes composed of aromatic polyamide thin films. Eviron. Sci. Techn. 35 (2001) 4334-4340.

[44] K.S. Kim, K.H. Lee, K. Cho, C.E. Park, Surface modification of polysulfone ultrafiltration membrane by oxygen plasma treatment. J. Membr. Sci. 199 (2002) 135-145.

[45] Y. Zhang, P. Liu, Polysulfone (PSf) composite membrane with micro-reaction locations (MRLs) made by doping sulphated TiO_2 deposited on SiO_2 nanotubes (STSNs) for cleaning wastewater. J. Membr. Sci. 493 (2015) 275-284.

[46] M. Kumar, Z. Gholamvand, A. Morrissey, K. Nolan, M. Ulbricht, J. Lawler, Preparation and characterization of low fouling novel hybrid ultrafiltration membranes based on the blends of GO-TiO_2 nanocomposite and polysulfone for humic acid removal, J. Membr. Sci. 506 (2016) 38-49.

[47] Y. Li, H. Jia, F. Pan, Z. Jiang, Q Cheng, Enhanced anti-swelling property and dehumidification performance by sodium alginate–poly(vinyl alcohol)/polysulfone composite hollow fiber membranes. J. Membr. Sci. 211 (2012) 407-408.

[48] J. Ma, M.H. Zhang, H. Wu, X. Yin, J. Chen, Z.Y. Jiang, Mussel-inspired fabrication of structurally stable chitosan/polyacrylonitrile composite membrane for pervaporation dehydration. J. Membr. Sci. 348 (2010) 150-159.

[49] J. Potreck, F. Uyar, H. Sijbesma, K. Nijmeijer, D. Stamatialis, M. Wessling, Sorption induced relaxations during water diffusion in S-PEEK. Phys. Chem. Chem. Phys. 11 (2009) 298-308.

[50] S.Y. Park, S.H. Choi, J.W. Chung, S.-Y. Kwak, Anti-scaling ultrafiltration/microfiltration (UF/MF) polyvinylidene fluoride (PVDF) membranes with positive surface charges for Ca^{2+}/silica-rich wastewater treatment. J. Membr. Sci. 480 (2015) 122-128.

[51] B. Agasanapura, R.E. Baltus, C.T. Tanneru, S. Chellam, Effect of electrostatic interactions on rejection of capsular and spherical particles from porous membranes: Theory and experiment. J. Colloid Interface Sci. 448 (2015) 492-500.

[52] N.S. Pujar, A.L. Zydney, Electrostatic and electrokinetic interactions during protein transport through narrow pore membranes. Ind. Eng. Chem. Res. 33 (1994) 2473-2482.

[53] M.M. Rohani, A.L. Zydney, Role of electrostatic interactions during protein ultrafiltration. Adv. Colloid Interface Sci. 160 (2010) 40-48.

[54] F. Yasar Mahlicli, S. Alsoy Altinkaya, Y. Yurekli, Preparation and characterization of polyacylonitrile membranes modified with polyelectrolyte deposition for separating similar sized proteins. J. Membr. Sci. 415-416 (2012) 383-390.

[55] V. Valiño, M. San Román, R. Ibañez, I. Ortiz, Improved separations of bovine serum albumin and lactoferrin mixtures using charged ultrafiltration membranes. Sep. Purif. Technol. 125 (2014) 163-169.

[56] R. Shang, A.R.D. Verliefde, J. Hu, Z. Zeng, J. Lu, A.J.B. Kemperman, H. Deng, K. Nijmeijer, S.G.J. Heijman, L.C. Rietveld, Tight ceramic UF membrane as RO pre-treatment: The role of electrostatic interactions on phosphate rejection. Water Res. 48 (2014) 498-507.

[57] P. Brandhuber, G. Amy, Arsenic removal by a charged ultrafiltration membrane-influences of membrane operating conditions and water quality on arsenic rejection. Desalination 140 (2001) 1-14.

[58] P. Brandhuber, G. Amy, Alternative methods for membrane filtration of arsenic from drinking water. Desalination 117 (1998) 1-10.

[59] C. Bellona, J.E. Drewes, The role of membrane surface charge and solute physico-chemical properties in the rejection of organic acids by NF membranes. J. Membr. Sci. 249 (2005) 227-234.

[60] L.D. Nghiem, A.I. Schäfer, M. Elimelech, Role of electrostatic interactions in the retention of pharmaceutically active contaminants by a loose nanofiltration membrane. J. Membr. Sci. 286 (2006) 52.

[61] A.R.D. Verliefde, E.R. Cornelissen, S.G.J. Heijmann, J.Q.J.C. Verberk, G.L. Amy, B. van der Bruggen, J.C. van Dijik, The role of electrostatic interactions on the rejection of organic solutes in aqueous solutions with nanofiltration. J. Membr. Sci. 322 (2008) 52-66.

[62] S. Alami-Younssi, A. Larbot, M. Persin, J. Sarrazin, L. Cot, Rejection of mineral saltson a gamma alumina nanofiltration membrane application to environmental process. J. Membr. Sci. 102 (1995) 123-129.

[63] J. Schaep, C. Vandecasteele, B. Peeters, J. Luyten, C. Dotremont, D. Roels, Characteristics and retention properties of a mesoporous γ-Al_2O_3 membrane nanofiltration. J. Membr. Sci. 163 (1999) 229-237.

[64] C. Labbez, P. Fievet, F. Thomas, A. Szymczyk, A. Vidonne, A. Poissy, P. Pagetti, Evaluation of the "DSPM" model on a titania membrane: measurements of charged and uncharged solute retention, electrokinetic charge, pore size, and water permeability. J. Colloid Interface Sci. 262 (2003) 200-211.

[65] E. Bet-Moushoul, Y. Mansourpanah, Kh. Farhadi, M. Tabatabaei, TiO_2 nanocomposite based polymeric membranes: A review on performance improvement for various applications in chemical engineering processes. Chem. Engin. J. 283 (2016) 29-46.

[66] Y. Mansourpanah, S.S. Madaeni, A. Rahimpour, A. Farhadian, A.H. Taheri, Formation of appropriate sites on nanofiltration membrane surface for binding TiO_2 photo-catalyst: Performance, characterization and fouling resistant capability. J. Membr. Sci. 330 (2009) 297-306.

[67] H.P. Ngang, B.S. Ooi, A.L. Ahmad, S.O. Lai, Preparation of PVDF–TiO_2 mixedmatrix membrane and its evaluation on dye adsorption and UV-cleaning properties, Chem. Eng. J. 197 (2012) 359–367.

[68] S. Neubert, D. Pliszka, V. Thavasi, E. Wintermantel, S. Ramakrishna, Conductive electrospun PANi-PEO/TiO_2 fibrous membrane for photocatalysis, Mater. Sci. Eng. B 176 (2011) 640–646.

[69] Y. Zhang, G. Zhang, S. Liu, C. Zhang, X. Xu, ''Naked'' TiO_2 capsulated in nonovoid microcapsule of poly (vinylidene fluoride) supporter with enhanced photocatalytic activity, Chem. Eng. J. 204–206 (2012) 217–224.

[70] O. Tahiri Alaoui, Q.T. Nguyen, C. Mbareck, T. Rhlalou, Elaboration and study of poly (vinylidene fluoride) – anatase TiO_2 composite membranes in photocatalytic degradation of dyes, Appl. Catal. A Gen. 358 (2009) 13–20.